9

Detection of Magnetic Phase in the Steam Generator Tubes of NPP

Duck-Gun Park, Kwon-Sang Ryu and Derac Son
KAERI, KRISS, Hannam Univiersity
Korea

1. Introduction

Steam generator tube (SGT) in nuclear power plant is a boundary between primary side and secondary side, whose integrity is one of the most critical factors to nuclear safety (Roberts, 1981). The SGT is made of nickel based Inconel alloy, which is composed of 75% Ni, 16.5%Cr and 8.15%Fe. Inconel alloy has very little magnetic response due to its austenitic nickel base, and the domain walls move relatively unimpeded through the material. The SGT are continuously exposed to harsh environmental conditions including high temperatures, pressures, fluid flow rates and material interactions resulting in various types of degradation mechanism such as corrosion, pitting, denting and inter granular attack. Multifrequency eddy current inspection techniques are currently among the most widespread techniques for the rapid inspection of SGT in nuclear power industry. Although the eddy current test (ECT) technique is adopted widespread in the nuclear industry (Bakhtiari, 1999), it has the limitation to size the flaw accurately because the eddy current measure the impedance signified by the conductivity change associated with the volumetric change of flaws, where the permeability of flaw is considered unity. The EC test currently applied in the nonferrous materials having relative permeability 1 such as Inconel alloy because the magnetic permeability of magnetic materials severely limits the depth of penetration of induced eddy currents. Furthermore, the small magnetic phase having permeability variation inherent in SGT can cause spurious EC test results (Park et al., 2010). It is well known that some part of SGT change as a magnetic phase known as permeability variation clusters (PVC) under the conditions of high pressure and temperature which is the operating environments of nuclear power plant. The relative permeability of the magnetic phase is greater than 1, and with a number of ferromagnetic metals, a value of several thousand can be reached. Internal stresses caused by drawing, straightening, or similar work on the material, can give rise to severe fluctuations in the permeability (Takahashi, 2004). These fluctuations would always cause interference with the test signals. In order to eliminate this interference effect during testing, the ferromagnetic test piece is magnetized by a suitable device such as magnetized ECT probe. Recently, to eliminate ECT signal fluctuation, the magnetized probe with the built-in permanent magnet is being used in the SG tube inspection, because a strong magnetic field of this probe reduces the variation of magnetic permeability, which gains S/N ratio. If we can separate magnetic phase (MP) selectively from the flaws using magnetic sensor, the reliability of EC in SGT inspection will

be greatly enhanced. This book begins with the introduction of steam generator, the creation mechanism of MP, the simulation, design and application of new probe which detect the MP. In section2 we present a brief recapitulation of the steam generator and the material properties of Inconel alloy, and ECT data containing the PVC obtained from nuclear power plant was analyzed, and also the hysteresis loop of PVC which is extracted from retired Kori-1 SG were measured. In section 3 we introduced the principle of new probe which separate the defects and MP, and the design of new probe in order to detect the MP and defects of SGT. In section 4 we performed electromagnetic analysis of MP using finite element simulation, and the results are compared with the experimental one which is obtained from our new probe.

2. Steam generator in pressurized water reactor

2.1 Overview of steam generator

Steam generator (SG) is the heat exchanger used to convert water into steam by using heat produced in a nuclear reactor core. The SGs also have an important safety role because they constitute one of the primary barriers between the radioactive and non-radioactive sides of the plant as the primary coolant becomes radioactive from its exposure to the core (Roberts, 1981). The function of the steam generator is to transfer the heat from the reactor cooling system to the secondary side of the tubes which contain feedwater. In commercial power plants SGs can measure up to 21 m in height and weigh as much as 800 tons. The layout of pressurized water reactor (PWR) components, and the structure of SG is shown in Fig. 1. Generally, 2~4 sets of SG were installed in the each nuclear power plant. Each SG can contain anywhere from 3,000 to 16,000 tubes, each about 20 mm in diameter. The coolant (treated water), which is maintained at high pressure to prevent boiling, is pumped through the nuclear reactor core. Heat transfer takes place between the reactor core and the

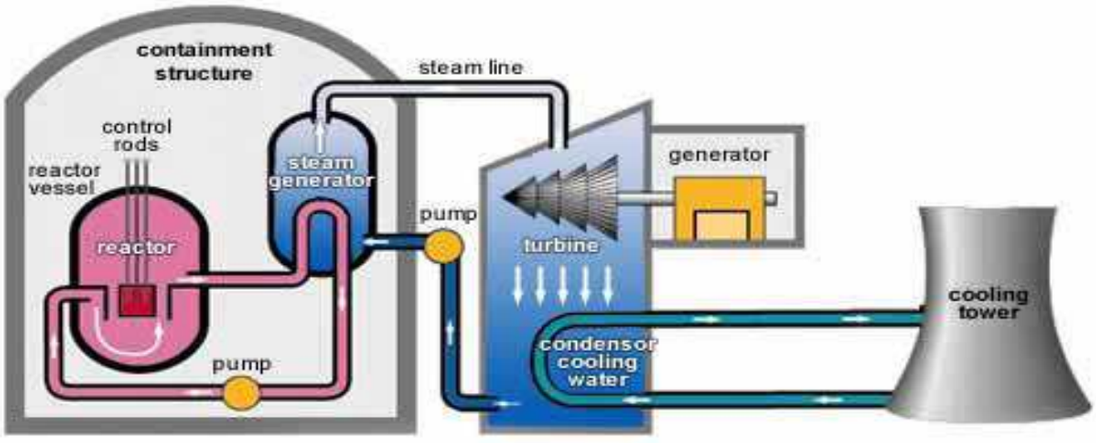

Fig. 1. The layout of pressurized water reactor (PWR) components, and structure of SG

circulating water and the coolant is then pumped through the primary tube side of the SG by coolant pumps before returning to the reactor core. This is referred to as the primary loop. As the feedwater passes the tube, it picks up heat and eventually gets converted to steam. That water flowing through the SG boils water on the shell side to produce steam in

the secondary loop that is delivered to the turbines to make electricity. The steam is subsequently condensed via cooled water from the tertiary loop and returned to the SG to be heated once again. The tertiary cooling water may be recirculated to cooling towers where it sheds waste heat before returning to condense more steam. Once through tertiary cooling may otherwise be provided by a river, lake, or ocean. This primary, secondary, tertiary cooling scheme is the most common way to extract usable energy from a controlled nuclear reaction. For this reason, the integrity of the tubing is essential in minimizing the leakage of water between the two sides of the plant. There is the potential that, if a tube bursts while a plant is operating, contaminated steam could escape directly to the secondary cooling loop. Radioactive releases can occur early in the event until the SG with the broken tube is isolated. Release paths include - air ejector exhaust and turbine driven emergency feed water pump exhaust normally; releases from the SG power operated relief valves may occur.

2.2 The degradation of SG and material specification

Two of the most important factors affecting a tube's vulnerability to degradation are the tube material and the tube's heat treatment. The two types of tube material being used in the PWR are Alloy 600 and Alloy 690 (Harrod et al., 2001). The chemical compositions of these materials are given in table 1. The two types of heat treatment applied to these materials for improving their mechanical and corrosion properties are mill annealing and thermal treatment. The SG tubes are either mill-annealed Alloy 600, thermally treated Alloy 600, or thermally treated Alloy 690. During the early-to-mid 1970s all plants, except one, had mill-annealed Alloy 600 steam generator tubes. The extensive tube degradation at PWRs with mill-annealed Alloy 600 SG tubes has resulted in tube leaks, tube ruptures, and midcycle SG tube inspections. This degradation also led to the replacement of mill-annealed Alloy 600 SGs at a number of plants and contributed to the permanent shutdown of other plants. There are known SGT damage mechanisms such as outer diameter stress corrosion cracking (ODSCC), pitting, volumetric changes, primary water stress corrosion cracking (PWSCC), and inter granular attack (IAG) (Okimura et al., 2006). The structure of SG and degradation mechanism is shown in Fig. 2. The dominant cause of tube degradation of Alloy 600 SGT was tube thinning. The cause of thinning is known as corrosion; therefore water chemistry flowing around them is treated as importantly. All plants have their water chemistry control programs virtually to eliminate the problem of tube thinning. After tube thinning, tube denting became a primary concern in the mid to late-1970s. Denting results from the corrosion of the carbon steel support plates and the buildup of corrosion product in the crevices between tubes and the tube support plates. Stress corrosion cracking (SCC) has primarily occurred at plants with mill-annealed Alloy 600 SGTs.

In the late 1970s, Alloy 600 tubes were subjected to a high-temperature treatment to improve the tube's resistance to corrosion. This thermal treatment process was first used on tubes installed in replacement SGs put into service in the early 1980s. Although no significant degradation problems have been observed in plants with thermally treated Alloy 600 SGTs, plants which replaced their SGs since 1989 have primarily used tubes fabricated from thermally treated Alloy 690, which is believed to be even more corrosion resistant than thermally treated Alloy 600. Traditional tube repair criteria are based on a minimum wall thickness requirement (USNRC, 2006). Typically, the tube wall thickness may be degraded by up to 40% of the initial wall thickness before the tube must be repaired. This allows an adequate margin against leakage and bursting. This criteria can be overly conservative for localized flaws such as short stress corrosion cracks. As a result, use of the 40% through-

wall repair criteria may result in tubes being unnecessarily removed from service even though they would continue to satisfy the existing regulatory guidance for adequate structural and leakage integrity. Most of the newer steam generators, including all of the replacement steam generators, have features which make the tubes less susceptible to corrosion-related damage. These include using stainless steel tube support plates to minimize the likelihood of denting and new fabrication techniques to minimize mechanical stress on tubes.

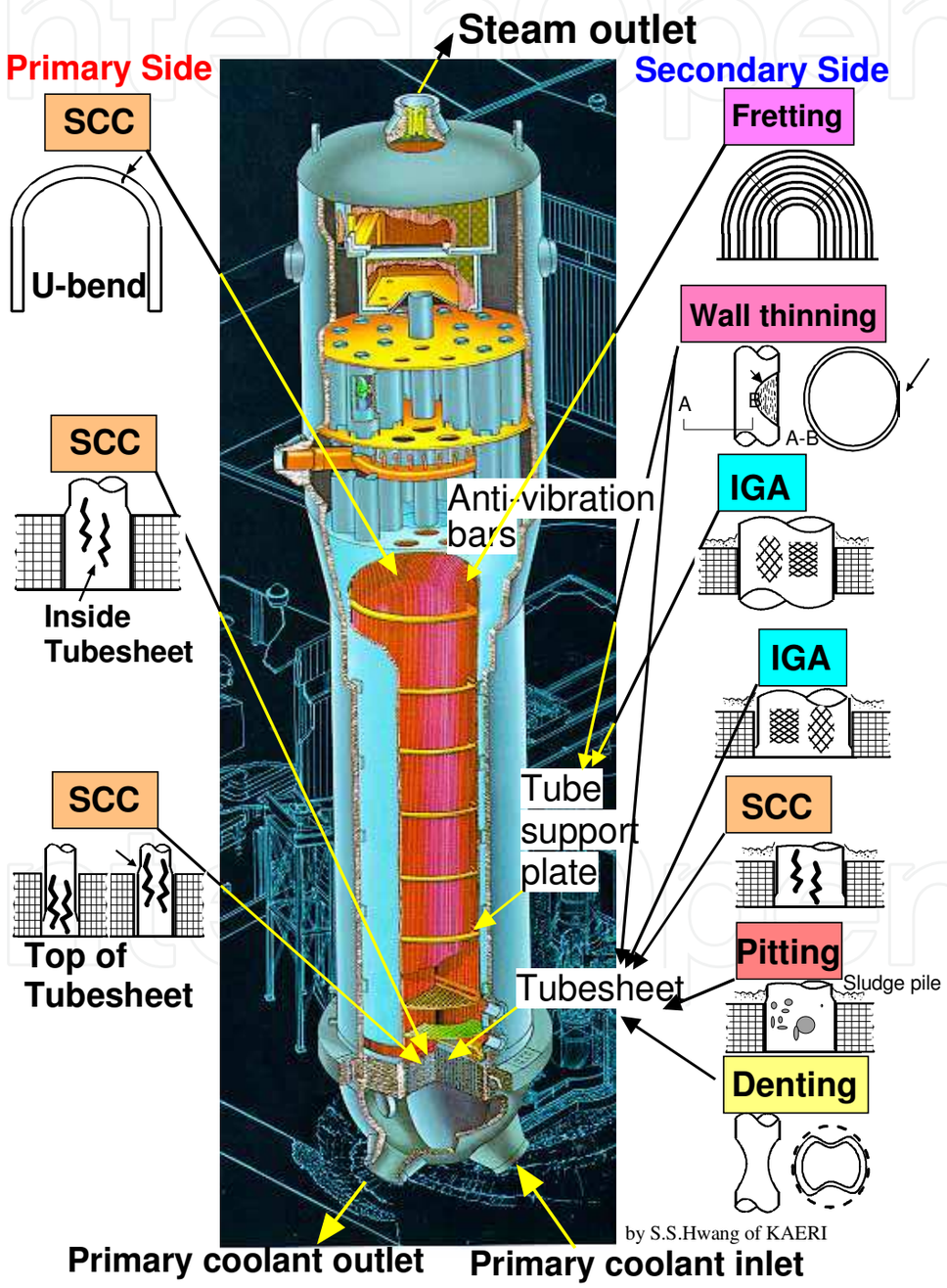

Fig. 2. The structure of SG and degradation mechanism

Material	Composition, wt%							
	Fe	Ni	Cr	C	Mn	Si	Al	Ti
I-600	8	72	15	.03	.2	.1	.2	.25
I-690	10	58	30	.02	.2	.1	.2	.25

Table 1. Chemical compositions (wt%) of Inconel 600 and Inconel 690

2.3 The inspection of SG

Since traditional inspection techniques only partially identified and precisely measured the size of cracks. The procedure performing comprehensive tube examinations must use appropriate inspection techniques and equipment capable of reliably detecting degradation, which is given in the code and standard (EPRI, 2010). The industry has since developed better methods of detecting cracks before tube integrity is potentially impaired. However, there continue to be challenges including precisely measuring crack size. Thus during scheduled maintenance outages or shutdowns, some or all of the steam generator tubes are inspected by ECT. Since the early days of commercial nuclear power, plant staffs at all plants have monitored the integrity of the SGTs using ECT during the normally scheduled refueling outages. If there is a thinning above a preset criterion or indications of abnormalities in the tubes, the tubes would be plugged or sleeved. Plugs prevent water from flowing through the tube. Sleeves may be used in those cases where defects or thinning might be present close to the tube sheet. Electric power research institute (EPRI) in US has supported industry efforts to improve steam generator reliability. A number of utilities have replaced their original steam generators. It is expected that during the 40 year initial operating license period, a plant may have to replace steam generators once. Excellent chemistry control on the secondary side of the steam generator is required. The ECT is the conventional method for inservice inspection (ISI) of SG tubing that is exposed to corrosive, high-pressure, and temperature environments. This nondestructive evaluation (NDE) method has advanced significantly over the years in all areas associated with probe design, instrumentation, and computer-aided data analysis (Sakamoto, 1993).

2.4 The problem of ECT

Although the EC technique is adopted widespread in the nuclear industry, it has the limitation like size the flaw accurately because the EC signal behavior depends on the total volume of flaw. Furthermore, PVC such as the build-up of magnetite (Fe_3O_4) and MP on the secondary side of the SG tubing has no direct effect on the tube integrity but it causes spurious EC test results (Kim et al., 2004). The relative permeability of the PVC is greater than 1, and with a number of ferromagnetic metals, a value of several thousand can be reached. Internal stresses caused by drawing, straightening or similar works on the material, creates the MP in the SG tube, which can give rise to several fluctuations in the permeability (Takahashi et al., 2004). These fluctuations would always cause interference with the test signals. Recently, to eliminate EC signal fluctuation, the magbias probe which the built-in permanent magnet being installed in the probe is used in the SG tube inspection, because of strong magnetic field of this probe reduces the variation of magnetic permeability, which gains S/N ratio (Song, 2006). However, the magbias ECT probe could not saturate strong PVC having large permeability, and the strong magnetic field of magnetized ECT probe amplifies the EC signal with noise by the interaction of magnetic field of ECT probe and

induced currents of probe coil. In this study, ECT data containing the PVC obtained from nuclear power plant was analyzed, and also the hysteresis loop of PVC which is extracted from retired Kori-1 SG were measured.

2.4.1 ECT signal fluctuation due to PVC (magnetic phase)

Fig. 3 shows inspection results by using the conventional probe and magbias probes. These signals are extracted from ECT data which is recorded as PVC signal by ECT examiner. The tubes were inspected by bobbin and motorized rotating probe coil (MRPC) probe with and without magnetized unit. The Fig.3 (a,b,c) represent the results of conventional bobbin and MRPC probe and Fig.3 (d,e,f) represent that of magbias probe. The MRPC probe consists of

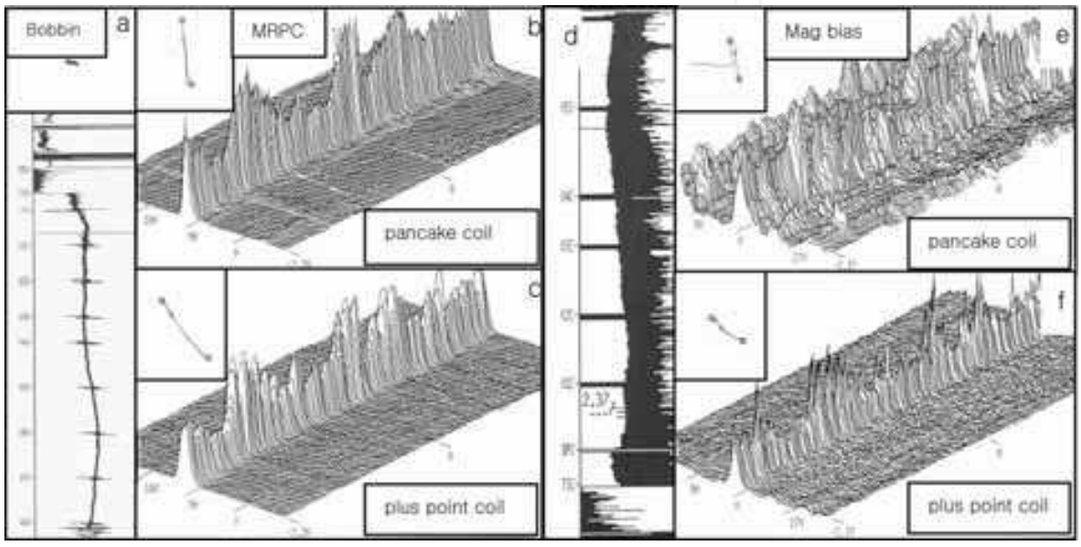

Fig. 3. The signal from (a) bobbin probe, (b) pancake coil (c) Plus point coil, and (d), (e), (f) represent the corresponding signals by magbias probe

three types of coils: two pancake and a +point. The pancake coils consist of two different diameters: 2.0 mm and 2.9 mm. The larger diameter pancake coil is to improve penetration depth of the signal to outside surface. Field experience shows that pancake coil has better sensitivity to volumetric defects whereas +point coil has better sensitivity to crack like defect (USNRC, 1996). Prior inspection of SG tube by bobbin probe indicates continuous distribution of PVC signal up to 1 m (Fig.3 (a, d)). However the PVC signal was not eliminated by magbias probe as shown in the left side of Fig. 3 (d, e, f), and the S/N ratio was reduced which is contrary to our expectation. The magnetized probe was introduced to saturate the ferromagnetic nature of PVC, but the saturation field depends on various factors such as demagnetization coefficient of the PVC. If the magnetic field of magnetized probe could not saturate the PVC, then the distortion of the ECT signals increases by the interaction of the magnetic field of magbias probe and PVC, which results low S/N ratio. The noise level by the +point coil was significantly decreased by the use of magbias probe. The data of the inspected tube shows the indication of long and narrow axial defects in bobbin and MRPC data. However, reevaluated results by magnetized probe shows that the data obtained from pancake coil covered with noise like signal and the data from plus point coil shows sharp ridge of mountain. The peak distribution obtained from pancake coil

considerably decreased and that from plus point coil disappeared by using the magnetized coil. The S/N ratio obtained from the bobbin and pancake of MRPC probe considerably decreased by using the magnbias probe, which suggests the flaw is constituted as a volumetric defect.

2.4.2 Confirmation of MP in SG

The samples for PVC in SG tube were extracted from retired SGT of Kori-1 NPP in Korea. Fig. 4 shows a permanent magnet attached on the fragment of SGT containing the PVC, which means that some parts of SG tube transformed as a MP. In order to investigate the magnetic properties of this PVC, the fragment was machined as rectangular type of 2 x 2 mm samples for measuring hysteresis loop using VSM. To confirm the mechanism of MP by deformation in Inconel alloy 600, the tensile tests were conducted in the room temperature and 600°C. The deformed area of tensile tested specimen was cut as a slice with 2 mm length for VSM measurement, and deformation rate was measured at each slice.

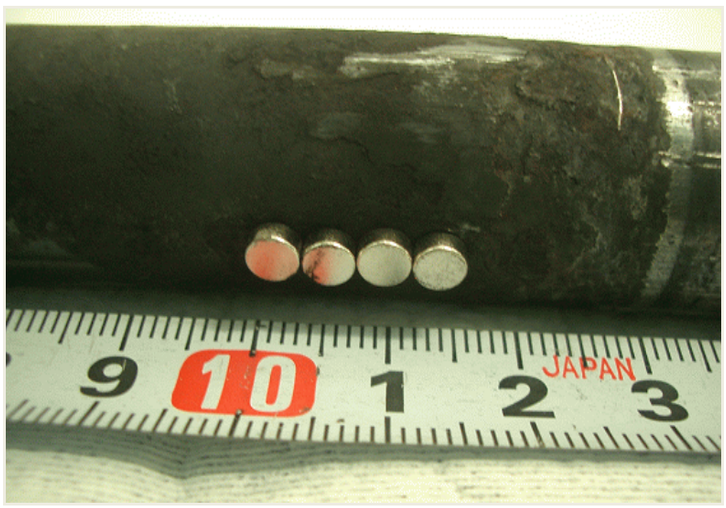

Fig. 4. The picture showing the substance of magnetic phase (PVC) in the SG tube. The sample was extracted from the retired SG tube of Kori-1 NPP

Fig. 5 shows the typical hysteresis loop of a fragment of PVC parts of SGT. The loop show different configuration for part by part of fragment. Although the sample is extracted from the same fragment, the magnetic moment and the coercivity shows different value with respect to sample position in the fragment. The onset of ferromagnetism in the high Cr and low Ni steels was associated with the formation of ferrite during sensitization. However, in higher nickel contents alloy such as Inconel 600, no ferrite formed and sensitization occurred without an increase in magnetic induction (Bain et al., 1993). For still higher Ni content in alloys, Curie temperature decrease rapidly with an increase in Cr content (Chevenard, 1934). Takahashi et al (Takahashi et al., 2004) proposed that the creation of MP in Inconel Alloy 600 is related with the decrease of Curie temperature by Cr depletion, however the permeability increase is less than 1.2 although the Cr content decreased from 17 to 14 wt% by depletion. These values are too small to form the hysteresis loop observed in Fig. 5. In order to identify the mechanism of PVC in the retired Kori-1 SG tube, the changes of hysteresis loop by deformation of Inconel 600 alloy were investigated.

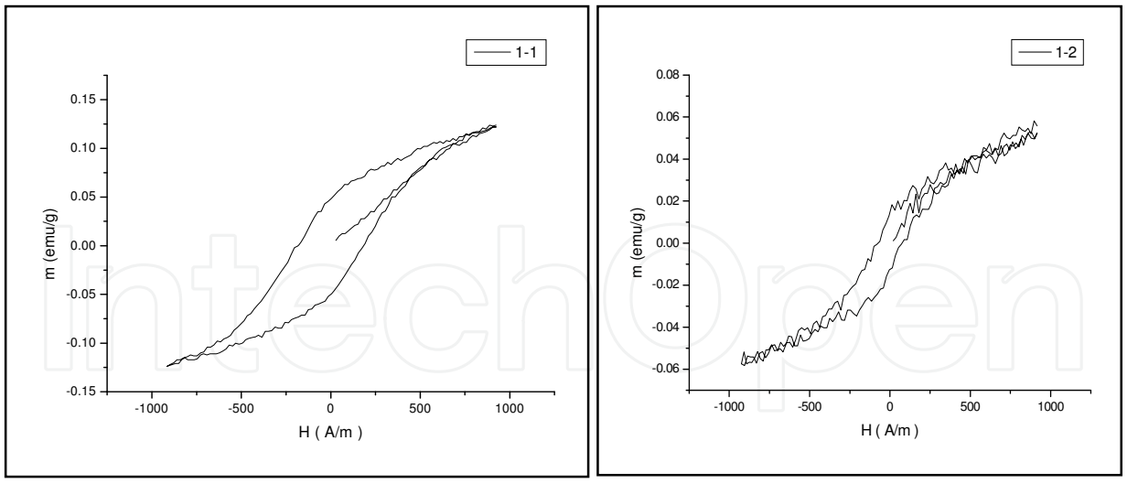

Fig. 5. The hystresis loop in the fragment of PVC parts of Kori-1 retired SG tube

Fig. 6 show the change of hysteresis loop for the specimen which are deformed at room temperature and 600 ◦C. The hystereis was not appeared in the annealed specimen at high temperature and tensile specimen tested at room temperature, but it was appeared in the tensile specimen tested at high temperature. The hysteresis of the specimen in the Fig. 6(b) cannot be explained as a Cr depletion, because it was not appeared in the undeformed specimen at high temperature. Therefore the MP can be created under the high temperature and pressure conditions, which is correspond to the stress corrosion cracking in the SG tube in the NPP (Bruemmer et al., 1981).

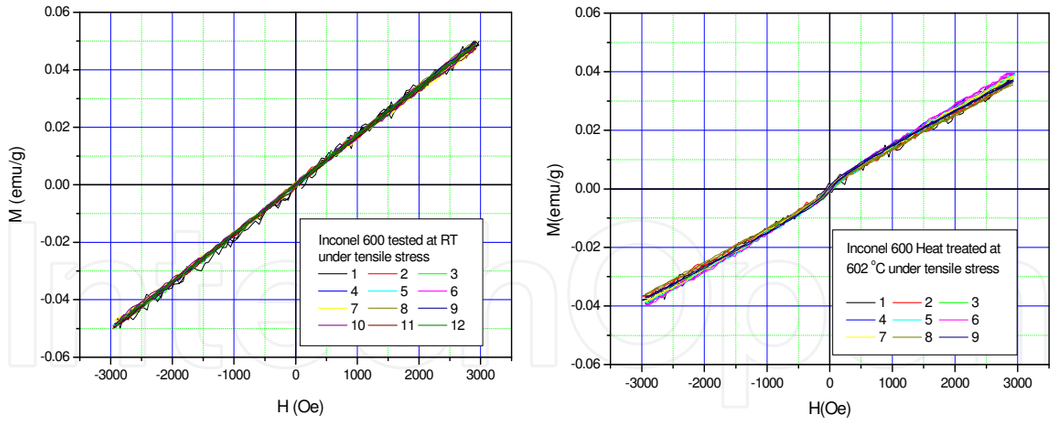

(a) (b)

Fig. 6. The hysteresis loop of the tensile tested specimen at room temperature (a), and tensile tested at high temperature (b)

3. Design and construction of sensor for MP measurement

Fig. 7 shows physical principle of ECT. When we measure impedance from applied voltage and current, there exist certain phase shift due to the resistance and inductance of coil as

shown in Fig. 7 (a). The phase will be changed by a defect as shown in Fig. 7(b). If we measure this phase, we could measure defects, and this is basic principle of ECT. But if there is defect in ferromagnetic material as shown in Fig. 7(d), we could not distinguish non-magnetic specimen without defect (Fig. 7(a)) and ferromagnetic specimen with defect. This is a critical problem, may be happen, flows generated in PVC of SGT.

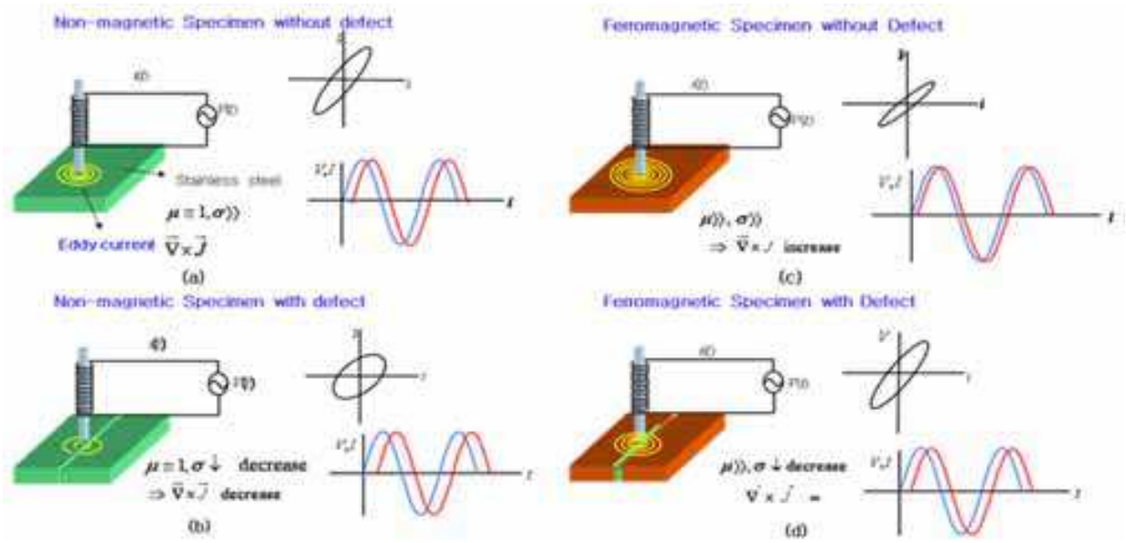

Fig. 7. Phase relationship between voltage and current of EC probe; (a) non-magnetic specimen without defect, (b) non-magnetic specimen with defect, (c) ferromagnetic specimen without defect, and (d) ferromagnetic specimen with defect

3.1 Fabrication of sensor

Fig. 8 shows the principle of the new probe which separates the defects and MP. U-shape of yoke was employed to magnetize test specimen and induced voltage from *B*-coil is proportional to the permeability of the specimen. To reduce lift-off effect, *H*-coil was used. The *H*-coil was connected to *B*-coil in series opposition. Fig. 9(a) shows dimension of the yoke and Fig. 9(b) shows photograph of the sensing yoke wound magnetizing coil, B-coil, and H-coil. As yoke material, 0.15 mm thickness of non-oriented silicon steel was used, and epoxy molded in vacuum. Using the thin gauged laminated core, we can magnetize yoke up to 10 kHz.

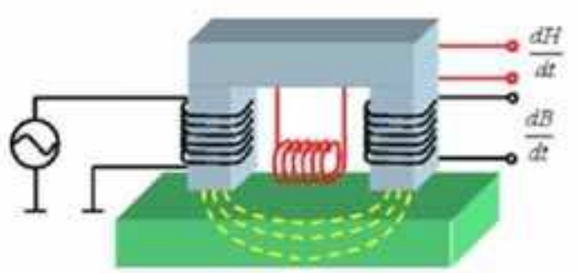

Fig. 8. Structure of the permeability sensor

Schematic diagram of the sensor electronics for signal processing is shown in Fig. 10. To measure amplitude variation and phase shift of induced voltage due to the magnetic reluctance change caused by the presence of magnetic phase and defects in the steam generator tube, two phase lock-in amplifier was employed, because magnetic permeability increase inductance of primary winding and phase angle between primary current and *B*-coil voltage will be increase, and vice verse in case of defects. To distinguish directions of

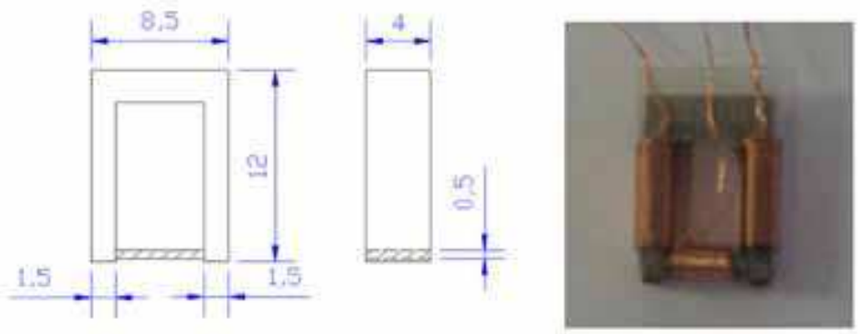

(a) (b)

Fig. 9. Dimension (a) and photograph (b) of U-shape sensing yoke

longitudinal and transverse defects, we have made two sensors and put into the probe with perpendicular each other. 4-channel analog signals(2-channel analog signal per sensor × 2 sensors) are converted to the digital signal using 4-channel input 16 bit ADC (Analog to Digital Converter), and the digital signals are transmitted to the personal computer through the RS232C interface using 8 bit embedded microcontroller. Fig. 11 shows photograph of front side and rear side of completed sensor. Diameter and length of the sensor were 16 mm and 200 mm respectively. Left hand side of front view of the probe, we can see two sensors one for longitudinal defect and the other for transverse defect. Fig. 12 shows developed scanning system and data acquisition software. Scanning of the sensor through the steam generator tube was controlled by stepping motor and motor controller, and software was programmed using LabVIEW (Son et al., 2009).

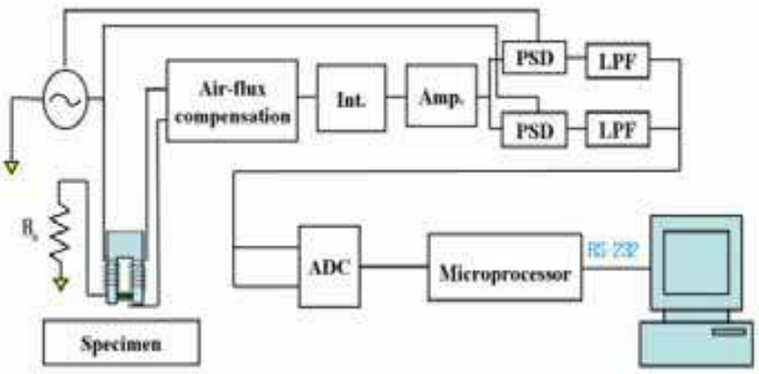

Fig. 10. Schematic diagram of the sensor system

Fig. 11. Photograph of the new probe, front side (above) and rear side (bottom)

Fig. 12. Photograph of the completed measuring system data acquisition software in PC and probe scanning system

3.2 Design of reference specimen

For the testing of the developed sensor for the defect detection of SG tube, we have made a reference specimen (RS) which consists of four kinds of artificial defects; defects located inside of tube, defects located outside of tube, and defects with and without ferromagnetic material. Fig.13 shows schematic diagram of constructed RS using Alloy600 in this work. The defects were machined with electrical discharge machining (EDM) method. Defects number 1, 2, 7, and 8 are located inside of tube and empty defect, and defects number 3, 4, 5, and 6 are located outside of tube are filled with ferromagnetic material in empty defects to demonstrate magnetic phase. Table 2 shows the dimension of the machined defects. Width and length of defects were fixed as 0.2 mm and 5 mm respectively, but depth of the defects was changed from 20% of the tube thickness (0.22 mm) to 80% of the tube thickness with step of 20%.

3.3 Experimental results

Fig. 14 shows the experimental results obtained by scanning of developed sensor using the reference specimen of Fig. 13. Here L_x means output voltage of in phase signal from longitudinal sensor, L_y output voltage of out of phase signal from longitudinal sensor, T_x output voltage of in phase signal from transverse sensor, T_y output voltage of out of phase signal from transverse sensor. From Fig. 14, we can see longitudinal sensor is sensitive to the longitudinal defects and signal amplitude is proportional to the defect size, and signals for MP (number 3,4,5,6,) are bigger than normal defects(number 1,2,7,8). Sign of x- and y-component signals are the same in case of MP but opposite in case of normal defects. For the case of transverse defects and MPs, sensor output voltage signals for the transverse reference specimen are shown in Fig. 15. Transverse sensor is sensitive to the transverse defects and MPs but not sensitive to the longitudinal defects and MPs. Signs of x- and y-component signals for the MPs and normal defects are the same as longitudinal defects. From Fig. 14 and Fig. 15, we can see that developed U-shape yoke sensor for SGT could detect not only MPs but also normal defects, and also distinguish longitudinal and transverse defects which are impossible with conventional bobbin type ECT.

Longitudinal and transverse defects				
Def.#	W	L	D	Remarks
1	0.2	5.00	0.213 (20 %)	Internal defects
2	0.2	5.00	0.427 (40 %)	
3	0.2	5.00	0.213 (20 %)	External defects PVC(1018)
4	0.2	5.00	0.427 (40 %)	
5	0.2	5.00	0.639 (60 %)	
6	0.2	5.00	0.852 (80 %)	
7	0.2	5.00	0.639 (60 %)	Internal defects
8	0.2	5.00	0.852 (80 %)	

Table 2. Dimension of defects in designed reference specimen

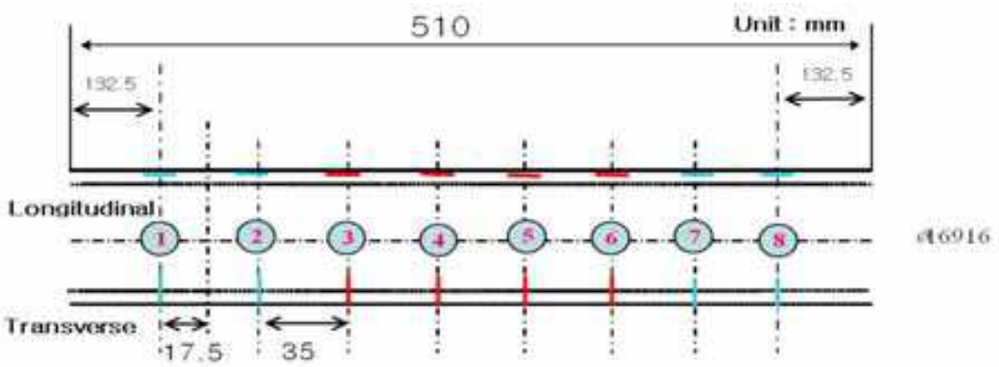

Fig. 13. Schematic diagram of reference specimen for the verification of developed sensor

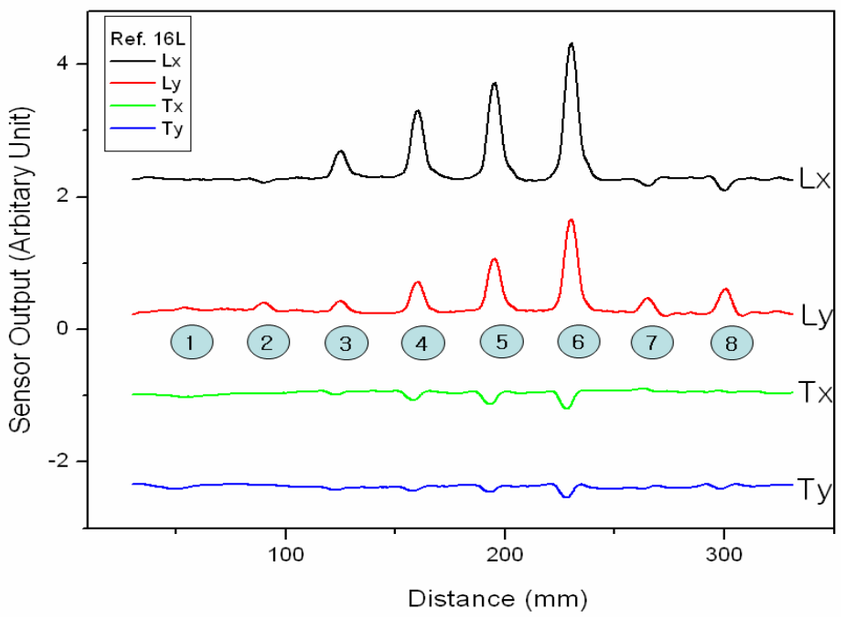

Fig. 14. Sensor output voltage signals from the longitudinal and transverse sensor for the longitudinal reference specimen

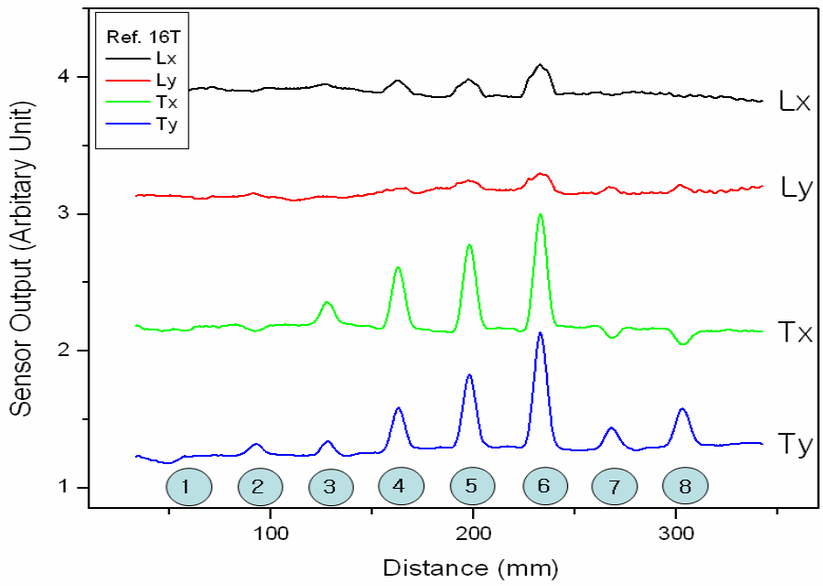

Fig. 15. Sensor output voltage signals from the longitudinal and transverse sensor for the transverse reference specimen

4. Magnetic field simulation

4.1 Manufacture of reference specimen

Fig. 16 (a) and (b) are the diagrams of the RS for testing a new designed sensor and simulating a magnetic field for longitudinal and circumferential MPs and defects. The inner diameter, the outer diameter, and the length of RS are 16.916 mmϕ, 19.05 mmϕ, and 440 mm, respectively. As shown Fig. 16 (a), the numbers 1, 2, 3, and 4 are longitudinal magnetic phase (LMPs) in the outer wall, while 5 and 6 are longitudinal defects (LDs) in the inner one (Ryu et al., 2010). As shown Fig. 16 (b), the numbers 1, 2, 3, and 4 are circumferential magnetic phases (CMPs) in outer wall, 5 and 6 are circumferential defects (CDs) in inner one (Ryu et al., 2010). The AISI 1810 steel was used to simulate the MPs. Magnetic properties were measured by hysteresis remagraph (Magnet-Physik), and conductivity was measured by using 4-point probe method (Janezic, 2004). The maximum permeability, coercivity, remanence, and conductivity of this steel are 9.80 x 10^{-4} H/m, 0.44 kA/m, 0.83 T, and 6.0 x 10^{5} S/m, respectively. Table 3 and 4 show the dimension and position of MPs and defects in the RS. The shape of MPs and defects is a hexahedron. The length and width of MPs and defects are the same, and the depth is deeper as the number increases.

The appearance of defects with outside ferrite sludge transforms the flow of magnetic flux because the EC is changed by the permeability of defects. Fig. 17 is a schematic diagram of the RS with outside ferrite sludge. The numbers 1, 2, 3, and 4 are inner defects, 5, 6, 7, and 8 are outer defects, 9, 10, 11 are inner defects, and 12 is penetration with outside ferrite sludge (Ryu et al., 2009). Table 5 shows the dimension and position of defects. Fig. 18 is a schematic diagram of the RS with nickel sleeving. The numbers 1, 2, 3, and 4 are inner defects with nickel sleeving. The thickness of nickel sleeving is 250 μm (Ryu et al., 2009). Table 6 shows the dimension of the artificial defects. The length and width are the same, only the depth is different.

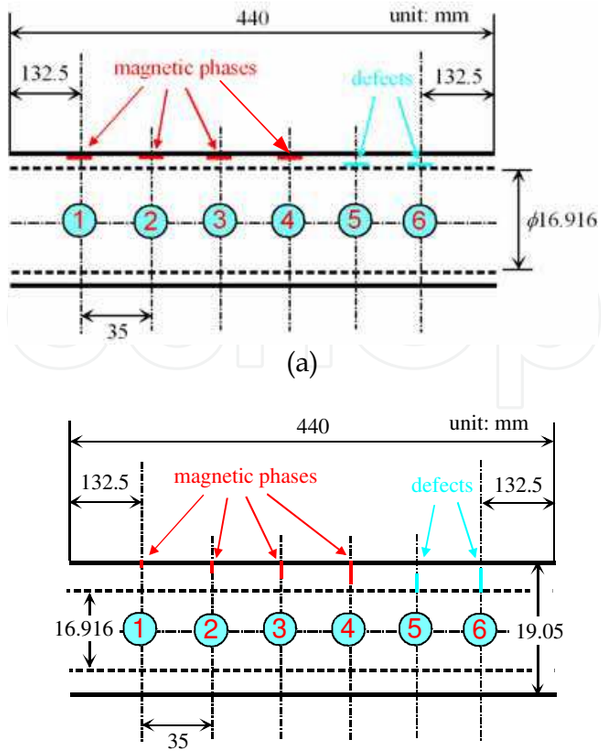

Fig. 16. Schematics of the RS for simulation of MPs and defects. (a) The numbers 1, 2, 3, and 4 are LMPs in the outer wall, while 5 and 6 are LDs in the inner one. (b) The numbers 1, 2, 3, and 4 are CMPs in the outer wall, while 5 and 6 are CDs in the inner one

Defect type	Defect No.	L (mm)	W (mm)	D (mm)
Outer defect (Insertion of MP)	1	5.00	0.20	0.213 (20%)
	2	5.00	0.20	0.427 (40%)
	3	5.00	0.20	0.639 (60%)
	4	5.00	0.20	0.852 (80%)
Inner defect	5	5.00	0.20	0.639 (60%)
	6	5.00	0.20	0.852 (80%)

Table 3. The dimension of the LMPs and LDs in the RS

Defect type	Defect No.	L (mm)	W (mm)	D (mm)
Outer defect (Insertion of MP)	1	5.00	0.20	0.213 (20%)
	2	5.00	0.20	0.427 (40%)
	3	5.00	0.20	0.639 (60%)
	4	5.00	0.20	0.852 (80%)
Inner defect	5	5.00	0.20	0.639 (60%)
	6	5.00	0.20	0.852 (80%)

Table 4. The dimension of the CMPs and CDs in the RS

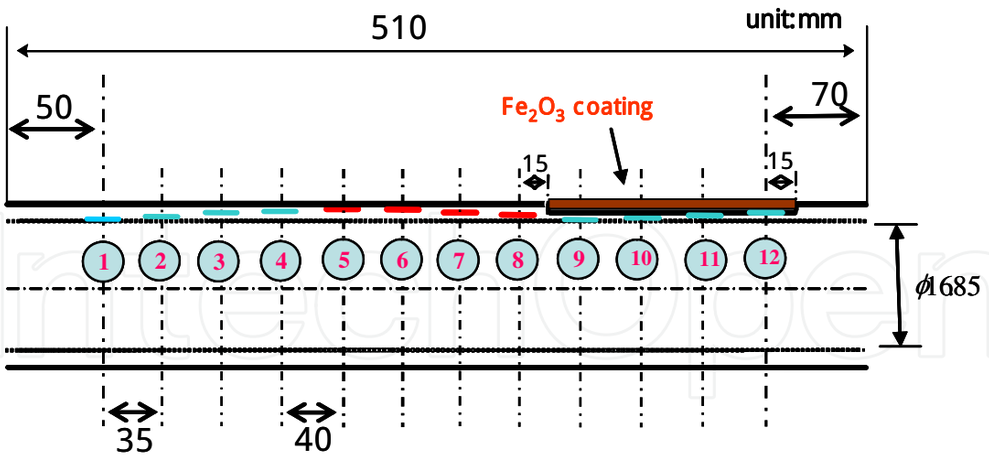

OD = 19.05 mm, ID = 16.85 mm, t = 1.10 mm

Fig. 17. Schematic diagram of RS. The number 1, 2, 3, and 4 are inner defects, 5, 6, 7, and 8 are outer defects, 9, 10, 11 are inner defects, and 12 is penetration with outside ferrite sludge

Defect type	Defect No.	L (mm)	W (mm)	D (mm)
Inner defect	1	10.00	0.20	0.22
	2	10.00	0.20	0.44
	3	10.00	0.20	0.66
	4	10.00	0.20	0.88
Outer defect	5	10.00	0.20	0.22
	6	10.00	0.20	0.44
	7	10.00	0.20	0.66
	8	10.00	0.20	0.88
Inner defect (30% cutting) + Fe_2O_3 coating	9	10.00	0.20	0.22
	10	10.00	0.20	0.44
	11	10.00	0.20	0.66
	12	10.00	0.20	penetration

Table 5. Dimension of defects with and without outside ferrite sludge

Defect No.	Width (mm)	Length (mm)	Depth (mm)	Note
1	0.20	10.00	0.25	Inner defect
2	0.20	10.00	0.51	
3	0.20	10.00	0.76	
4	0.20	10.00	1.02	

Table 6. Dimension of defects in designed RS sleeved by nickel

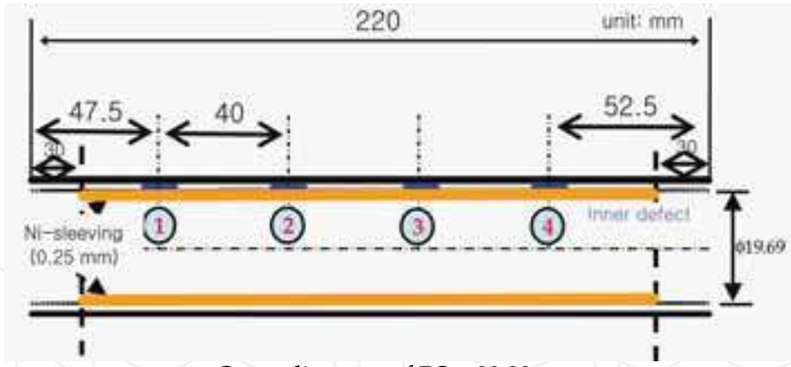

Outer diameter of RS = 22.33 mm
Inner diameter of RS = 19.69 mm
Thickness of RS = 1.32 mm
Interval of defects = 40 mm

Fig. 18. Schematic diagram of RS with nickel sleeving. The numbers 1, 2, 3, and 4 are inner defects in nickel sleeving

4.2 Magnetic field simulation

The Ansoft Maxwell V12 3D software was used for calculating the reactance change caused by the presence of MPs and defects (Ansoft Corp., 2009). The *U*-type probe, which has two kinds of coils perpendicularly stands on the Inconnel tube including the MPs and defects. The solver for the FEM was the eddy current. The magnetic potential applied to the magnetizing coil was 10 A·turn, the frequency was 10 kHz. Fig. 19 shows the mesh configuration for simulating the reactance change of (a) LMPs and LDs, and (b) CMPs and CDs. The mesh size of LMPs and LDs was about 280,000 tetrahedra, and one of CMPs and

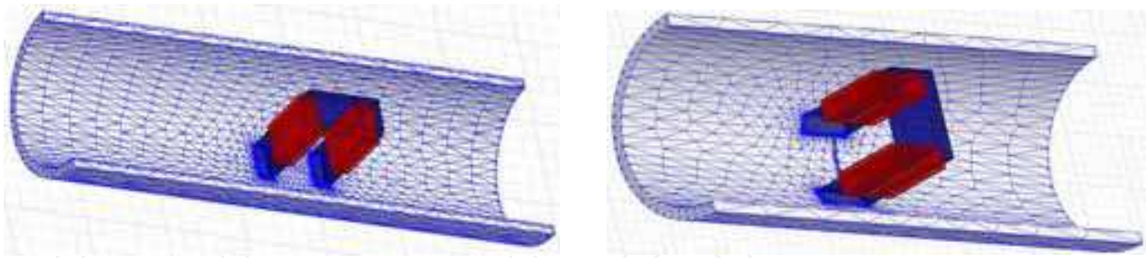

(a) (b)

Fig. 19. Mesh configuration for simulating the reactance change of (a) LMPs and LDs, (b) CMPs and CDs

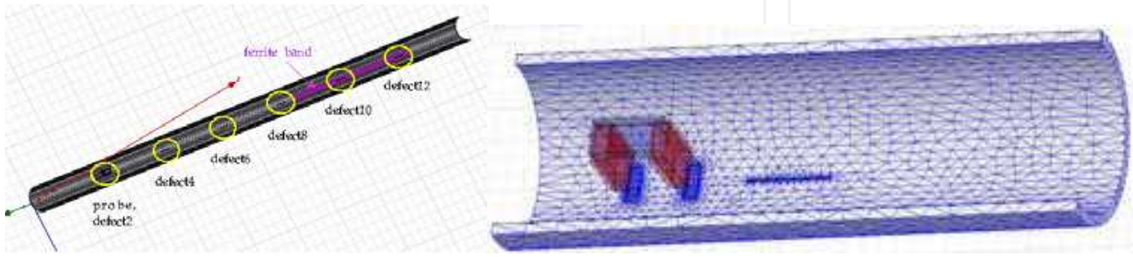

(a) (b)

Fig. 20. (a) FEM model with outside ferrite sludge and (b) mesh configuration for simulating the reactance

CDs was about 260,000 tetrahedra. Fig. 20 shows (a) the FEM model, and (b) the mesh configuration of the defect with outside ferrite sludge. The size of the mesh was 291,000 tetrahedra. Figure 21 shows (a) the FEM model for LDs in Inconel tube with nickel sleeving, and (b) the mesh configuration of the defect sleeved by nickel. The solver of FEM was eddy current, the number of mesh was 364,000 tetrahedra.

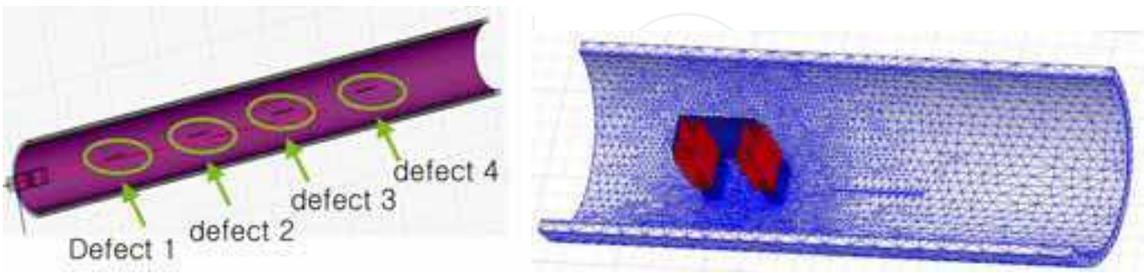

(a) (b)

Fig. 21. (a) FEM model for LDs in Alloy600 tube with nickel sleeving, and (b) mesh configuration of the defect with nickel sleeving for simulation

4.3 Results and discussions

The calculated results by the FEM for LMPs and LDs are shown in Fig. 22(a), and sensor output is shown in Fig. 22(b). As shown in Fig. 22, the reactance amplitude increases with increasing depth of the inner LMP and outer LD (Ryu, 2010). The symbols are the reactance simulated by FEM, and the solid line, without symbols, is the reactance measured of the fabricated sensor (Son, 2009). The amplitude of signals at the LMPs and LDs increase with deepening depth, but the phase of signals is the opposite. So the new sensor can distinguish the LMPs and LDs produced in SGT.

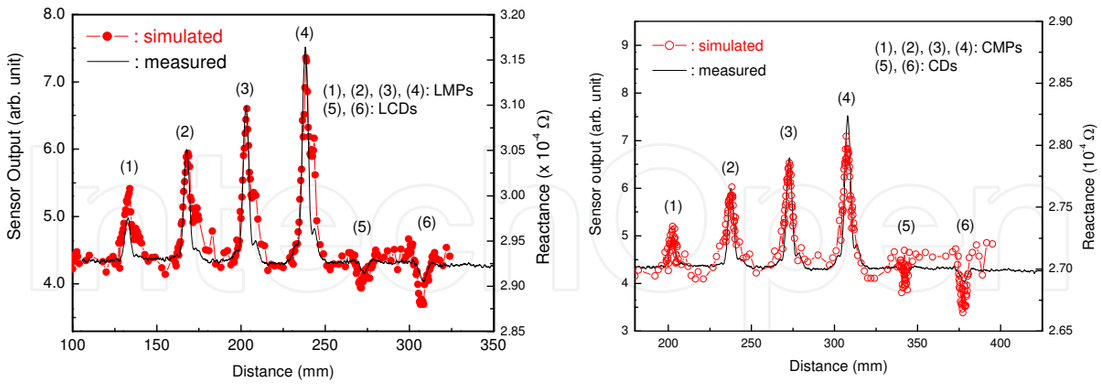

(a) (b)

Fig. 22. Reactance simulated by FEM and output measured by manufactured sensor for (a) LMPs and LDs, (b) CMPs and CDs. The numbers 1, 2, 3, and 4 are LMPs, 5 and 6 are LDs at (a), and the numbers 1, 2, 3, and 4 are CMPs, 5 and 6 are CDs at (b)

The results calculated by the FEM and the in-phase x-output of sensor for CMPs and CDs are shown in Fig. 22(b). As shown in figure 22(b), the reactance amplitude increases with increasing depth of the outer CMP and inner CD (Ryu, 2010). The symbols are the reactance

simulated by FEM, the solid line, without symbols, indicates the reactance change measured of the fabricated sensor. The amplitude of signals at the CMPs and CDs increase with depth, but the phase of signals is opposite each other. So the new sensor can measure CMPs and CDs, and also distinguish the CMPs and CDs produced in SGT by phase.

The result simulated by FEM and the output measured by fabricated sensor for RS with and without outside ferrite sludge are shown in Fig. 23(a). The reactance amplitude increases with increasing depth of the inner and outer defect (Ryu, 2009). It jumps when there is outside ferrite sludge because the reactance is affected by the permeability of the ferrite sludge. Also, it increases with increasing depth, and is much stronger for passed through defect. The measured signal at the *B*-sensing coil is composed of a resistance (real part) and a reactance (imaginary part). Using this, we calculated the reactance of the *B*-sensing coil. The solid line, without symbols, indicated the reactance measured (Ryu, 2009). Fig. 23(b) shows the output of fabricated sensor and the calculated reactance for defects in Alloy tube with nickel sleeving. As shown in Fig. 23(b), the reactance amplitude increases with deepening depth of defect (Ryu, 2009). The defect 1 was not measured, because the distance from the end of the specimen to defect 1 is very short. The measured signal at *B*-sensing coil is composed of resistance (real part) and reactance (imaginary part), we calculated the reactance of *B*-sensing coil. The reactance amplitude calculated for the defect present in the reference Alloy 600 tube is well agreeable with the results measured by the fabricated probe.

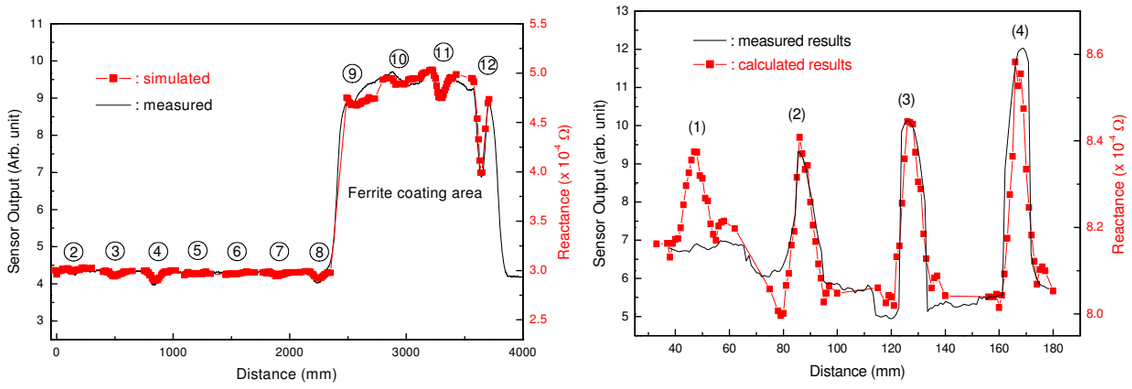

(a) (b)

Fig. 23. Reactance simulated by FEM and output measured by manufactured sensor for (a) with and without outside ferrite sludge, (b) with nickel sleeving. The numbers from 2 to 8 are LMPs, from 9 to 12 LMPs with outside ferrite sludge at (a), and the numbers 1, 2, 3, and 4 are LMPs with nickel sleeving at (b)

5. Conclusion

The degradation and materials specification of SGT were reviewed, and the limitation of ECT was designated. The effects of magnetic phase on ECT signal were analyzed using the inspection data of NPP. The large coercivity and clear hystersis loops of PVC which is extracted from the retired SG tubes of Kori-1 NNP are cannot be explained as a decrease of Curie temperature by Cr depletion. The hysteresis loop which is observed in the tensile tested specimen at high temperature suggests that the MP created in the SG tube is related with stress corrosion cracking. To separate the MP and defect using one sensor, new kind of

probe which measure permeability change of the specimen was developed. Using the new probe and RS which has MP and normal defect, we could measure and distinguish not only MP but also normal defect, and also distinguish longitudinal and transverse defects which are impossible with conventional bobbin type ECT probe. The reactance change of various MPs and defects was calculated by FEM simulation, and the results were compared with measured value by new probe. The reactance increased with increasing depth of the LMPs, CMPs, LDs and CDs, but the phase of signals at the MPs and defects are the opposite. The reactance increased with increasing depth of the defect with and without outside ferrite sludge. But it jumps when there is outside ferrite sludge, and is much stronger for passed through defect. The reactance increased with deepening the depth of the defect with nickel sleeving. The reactance calculated for the MPs and defects in the Alloy600 tube agrees with the result measured by the sensor. So the new sensor can distinguish the MPs and defects produced in SGT by phase change.

6. References

Ansoft Corp.; (2009), http://www.ansoft.com.

Bain, E. C. Aborn, R. H. & Rutherford, J. J. (1933).*Trans. ASM*. Vol. 21, (Month & Year) 481.

Bakhtiari, S. (1999). Advanced Eddy Current NDE for Steam Generator Tubing, ANL/ET/CP-98667

Bruemmer, S.M.; Charlot, L.A. & Henager, C.H. (1988). *Corrosion*, 782

Chevenard, P. (1934). *C.R. Acad. Sci.* Vol. 198, pp.1144.

EPRI; (2010), 2010 Portfolio PWR Steam Generator Management Program Overview 41.01.02

Hwang, S.S.; Kim, H.P. Kim, J.S. (2003). Corrosion degradation of steam generators in Korea, *Proc. Of SMiRt 17*, Czech Republic (Agu. 17-22), Prague.

Harrod, D.L. Gold, R.E. & Jacko, R.J. (2001). Alloy Optimization for PWR Steam Generator Heat-Transfer Tubing, *JOM Journal of the Minerals, Metals and Materials Society*, Vol. 53, No.7, (July 2001), pp.14-17

Jackson, L.R. & Russel, H.W. (1938). *Instruments*. Vol. 11, pp.280

Janezic, M. D.; (2004). DC Conductivity Measurements of Metals, *NIST Technical Note*, 1531.

Kim, Y. H. Song, S. J. Heo, J. S. Lee, H. B. & Song, M. H. (2004). *Key Engineering Materials*. Vol. 555, pp. 270-273,

Okimura, K. Hori, N. Mukai, M. Masumoto, K. Kamo, K. & Kurokawa, M. (2006). Mitsubish Heavy Industries Technical Review. Vol. 43, No. 4, (Dec. 2006).

Park, D.G. Ryu, K.S. Son, D. & Cheong, Y.M. (2010). Effects of magnetic phase on the ECT signal in the SG tubes, *IEEE-Trans. Mag*. Vol. 46, No. 2, (Feb. 2010), pp.560-562.

Roberts , J.T. A. (1981). Structural Materials in Nuclear Power Systems, Plenum Press, New York,

Ryu, K. S. Son, D. Park, D. G. Jung, J. K. & Kim, Y. I. (2009). Reactance simulation for the defects in steam generator tube woth outside ferrite sludge, *J Appl. Phys.*, Vol. 105, No. 7, (March 2009), pp. 07E712-1 (3 pages).

Ryu, K. S. Son, D. Park, D. G. & Jung, J. K. (2009). Reactance change at defect in inconel tube with nickel sleeving, *IEEE Trans. Magn*, Vol. 45, No.6, (June2009, pp. 2733-2735

Ryu, K. S. Son, D. Park, D. G. Jung, J. K. & Kim, Y. I. (2010). Magnetic field simulation of magnetic phase detection sensor for steam generator tube in nuclear power plants. *J Appl. Phys*,Vol. 107, No.9, (May 2010), pp.09E704-1 (3 pages).

Sakamoto, T.; (1993) *Journal of the Japanese Society for Non-destructive Inspection*. Vol.42, No. 9
Son, D., Joung, W., Park, D., Ryu,K., (2009). *J of Magnetics*. Vol. 14, No. 2, pp. 97.
Son, D. Joung, W. Park, D. G. Ryu, K. S. (2009). Magnetic sensor for the defect detection of steam generator tube with outside ferrite sldge, *IEEE Trans on Magnetics*. Vol. 45, No. 6, (June 2009), pp. 2724-2726.
Son, D. Joung, W. I. Park, D. G. Ryu, K. S. (2009). *J of Magnetics*, Vol. 14, No. 2, pp.90.
Song, S. C. Lee, Y.T. Jung, H.S. & Shin, Y.K. (2006). *J Kor. Soc. NDT*. Vol. 26, No. 3, pp.174.
Strauss, B. Schotty, H. & Hinnueber, J. (1930). *Z. Anorg. Allg. Chem*. Vol.18, No.1, (March 1930), pp. 309-324.
Takahashi, S. Sato, Y. Kamada, Y. Abe, T. (2004). Study of chromium depletion by magnetic method in Ni-based alloys, *J Magn. Magn. Mater*. Vol. 269,No.2, (Feb 2004), pp. 139-149.
Takahashi, S. Sato, H. Kamada, Y. Ara, K. & Kikuchi, H. (2004). A new magnetic NDE method in inconel 600 alloy, *International Journal of Applied Electromagnetics and Mechanics*, Vol. 19, No. 1-4, (April 2004), pp.3-8.
USNRC; (2006) NEI97-06, Related documents and other resources, http://www.nrc.gov
USNRC; (1996), Steam Generator Tube Failures, NUREG/CR-6365

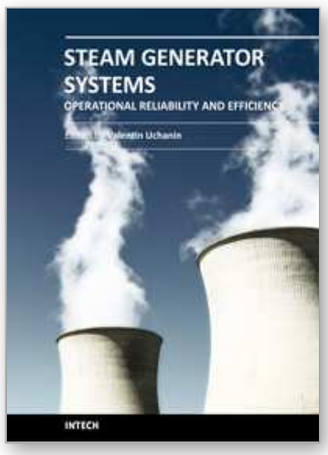

Steam Generator Systems: Operational Reliability and Efficiency
Edited by Dr. Valentin Uchanin

ISBN 978-953-307-303-3
Hard cover, 424 pages
Publisher InTech
Published online 16, March, 2011
Published in print edition March, 2011

The book is intended for practical engineers, researchers, students and other people dealing with the reviewed problems. We hope that the presented book will be beneficial to all readers and initiate further inquiry and development with aspiration for better future. The authors from different countries all over the world (Germany, France, Italy, Japan, Slovenia, Indonesia, Belgium, Romania, Lithuania, Russia, Spain, Sweden, Korea and Ukraine) prepared chapters for this book. Such a broad geography indicates a high significance of considered subjects.

How to reference
In order to correctly reference this scholarly work, feel free to copy and paste the following:

Duck-Gun Park, Kwon-Sang Ryu and Derac Son (2011). Detection of Magnetic Phase in the Steam Generator Tubes of NPP, Steam Generator Systems: Operational Reliability and Efficiency, Dr. Valentin Uchanin (Ed.), ISBN: 978-953-307-303-3, InTech, Available from: http://www.intechopen.com/books/steam-generator-systems-operational-reliability-and-efficiency/detection-of-magnetic-phase-in-the-steam-generator-tubes-of-npp

INTECH
open science | open minds

InTech Europe
University Campus STeP Ri
Slavka Krautzeka 83/A
51000 Rijeka, Croatia
Phone: +385 (51) 770 447
Fax: +385 (51) 686 166
www.intechopen.com

InTech China
Unit 405, Office Block, Hotel Equatorial Shanghai
No.65, Yan An Road (West), Shanghai, 200040, China
中国上海市延安西路65号上海国际贵都大饭店办公楼405单元
Phone: +86-21-62489820
Fax: +86-21-62489821

IntechOpen